Supplementary materials for

Double hysteresis loop in synchronization transitions of multiplex networks: the role of frequency arrangements and frustration

Ali Seif[1] and Mina Zarei[1,*]

[1]Institute of Advanced Studies in Basic Sciences (IASBS), Department of Physics, Zanjan, 45137-66731, Iran.

February 27, 2025

This supplementary material provides explanations for supplementary figures SF1–SF8 and supplementary videos SV1–SV3.

Description of Supplementary Figures

Description of Figure SF1:

This figure presents a comparative analysis of phase transitions in a Regular frequency assignment model for $\alpha = 0$ and $\alpha = \frac{\pi}{2}$, focusing on the synchronization dynamics within layer II. The synchronization phase transition is depicted for both forward and backward paths across the entire layer (blue), as well as for the left (green), middle (black), and right (red) sections.

For $\alpha = 0$ (panels **a-d**), the observed discontinuous jumps in synchronization are primarily associated with the peripheral sections, where nodes exhibit frequency differences compared to their mirror counterparts in the opposite layer. The middle section, in contrast, transitions smoothly and reversibly between incoherent and coherent states.

For $\alpha = \frac{\pi}{2}$ (panels **e-h**), the first transition corresponds to the synchronization of the middle section, where nodes share identical frequencies with their mirror counterparts. The second transition, marked by a hysteresis loop, is associated with the synchronization of the left and right sections, where nodes have frequency mismatches with their mirrored nodes. Unlike the $\alpha = 0$ case, the synchronization process here is characterized by discontinuous and irreversible transitions in both the middle and peripheral sections.

The insets in each panel provide a magnified view of the transition regions, emphasizing the abrupt nature of the phase transitions. This detailed comparison highlights the distinct synchronization behaviors induced by frustration ($\alpha = \frac{\pi}{2}$) in contrast to the frustration-free case ($\alpha = 0$).

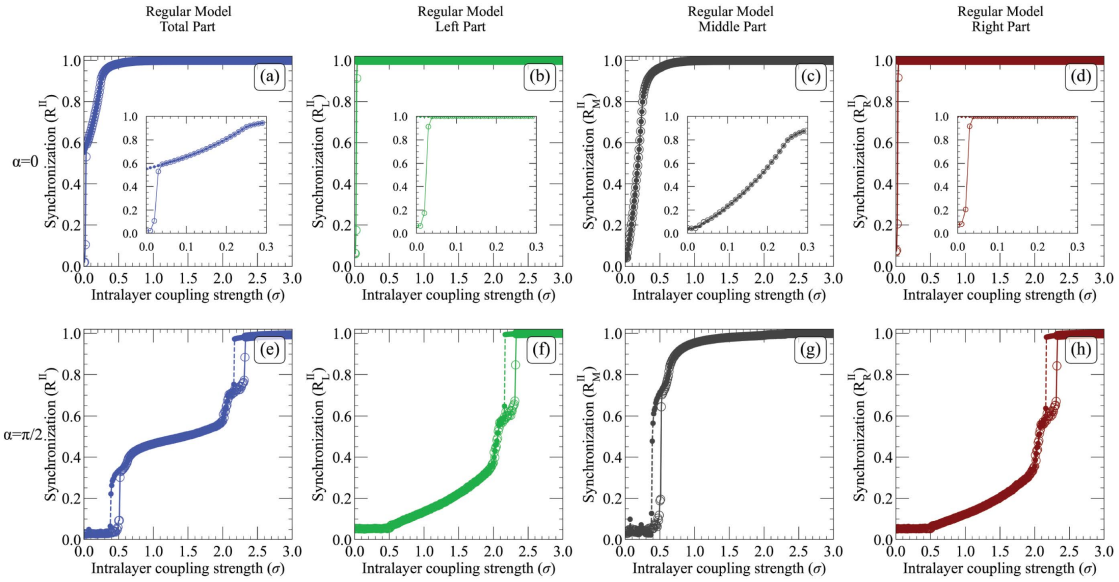

Figure SF 1: Comparison of phase transitions in the Regular frequency arrangement model for $\alpha = 0$ and $\alpha = \frac{\pi}{2}$, highlighting hysteresis loops. (**a-d**) Phase transition curves for the entire layer, as well as the left, middle, and right sections of layer II with $\alpha = 0$. (**e-h**) Corresponding phase transition curves for $\alpha = \frac{\pi}{2}$. The insets in the first row provide a magnified view of the transition regions, emphasizing the first-order phase transitions. Solid lines with unfilled points denote forward transitions, while dashed lines with filled points represent backward transitions. The parameters used are $\Delta\omega = 0.8$ and $\lambda = 10$.

Description of Figure SF2:

This figure highlights the impact of interlayer interactions on synchronization dynamics in the absence of a phase lag ($\alpha = 0$) within layer II. The synchronization curves in panel (**a**) illustrate the transition behavior of the entire layer, as well as its left, middle, and right sections. Notably, during the backward transition, the peripheral sections remain synchronized even when the intralayer coupling strength is reduced to zero ($\sigma = 0$), a consequence of the persistent interlayer interactions.

Panels (**b**) to (**e**) present the instantaneous phase similarity matrices ($S_{ij}^{II}(t) = \cos\left(\theta_i^{II}(t) - \theta_j^{II}(t)\right)$) along the backward path for different values of σ: (**b**) $\sigma = 0.5$, (**c**) $\sigma = 0.25$, (**d**) $\sigma = 0.15$, (**e**) $\sigma = 0$.

At higher intralayer coupling values, the network approaches full synchronization. However, as σ decreases, the middle section—where nodes have zero frequency differences with their mirror counterparts—gradually desynchronizes, whereas the left and right sections retain their synchronization even at $\sigma = 0$. This behavior underscores the role of interlayer coupling in sustaining the coherence of peripheral regions. The Regular frequency assignment model was utilized in this analysis.

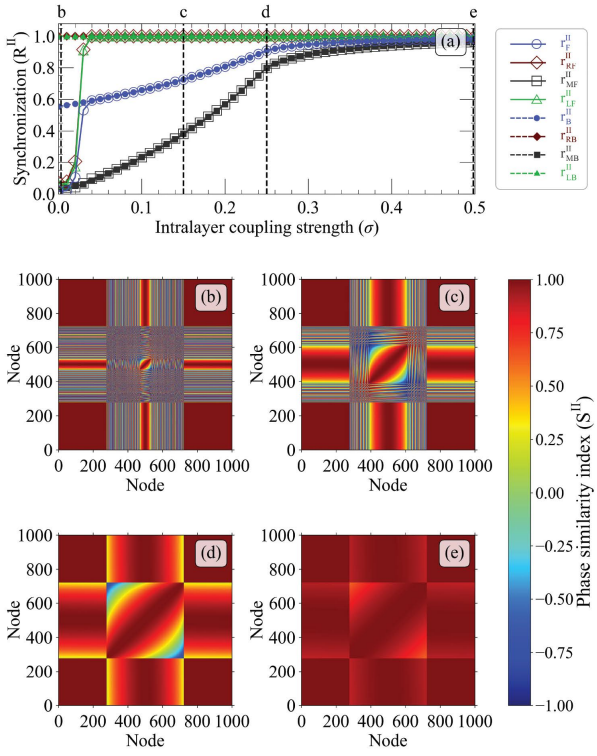

Figure SF 2: Comparative analysis of synchronization dynamics in layer II for the Regular model with $\alpha = 0$. (**a**) Phase synchronization curves as a function of coupling strength for the entire layer (blue circles), left section (green triangles), middle section (black squares), and right section (red diamonds). Open markers represent forward transitions, while filled markers indicate backward transitions. (**b-e**) Instantaneous phase similarity matrices for different values of coupling strength in the backward path: (**b**) $\sigma = 0$, (**c**) $\sigma = 0.15$, (**d**) $\sigma = 0.25$, and (**e**) $\sigma = 0.5$. Parameters are $\Delta\omega = 0.8$ and $\lambda = 10$.

Description of Figure SF3:

This figure illustrates that when the synchrony signals of the left and right sections (**a**) are separated by frequency, the low-frequency oscillations (LFOs) of both sections are in-phase (**b**), whereas the medium-frequency oscillations (MFOs) are in anti-phase (**c**). This analysis employed for a Regular model frequency assignment.

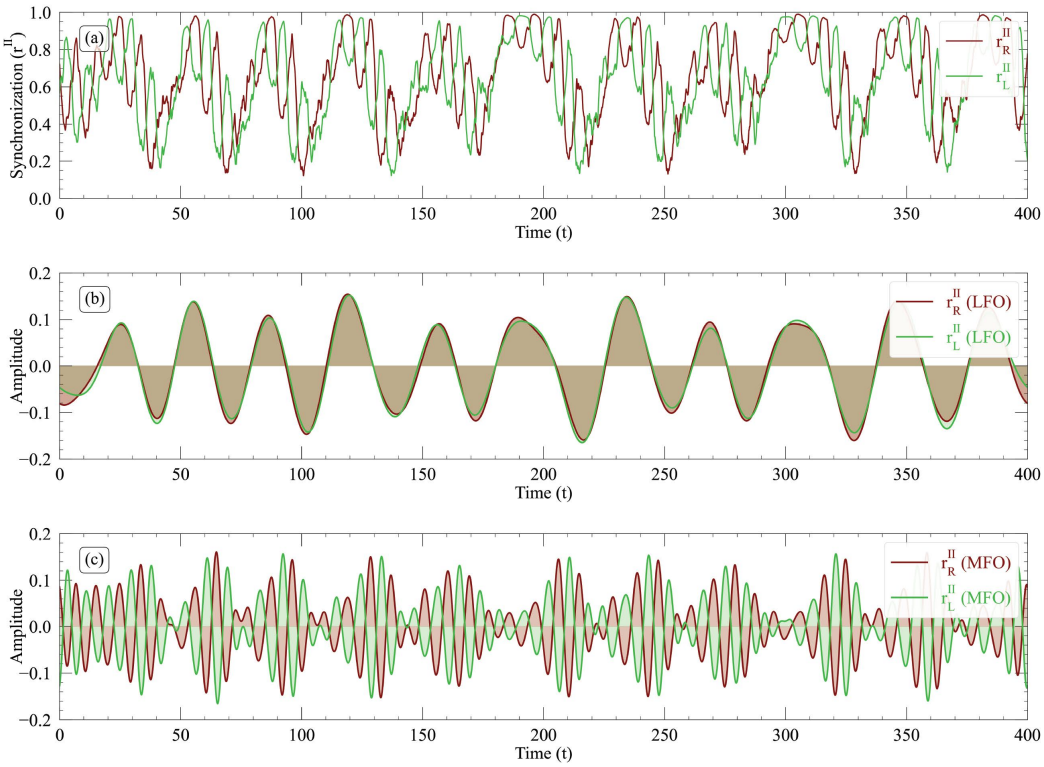

Figure SF 3: Phase similarities of synchronization order parameters in the left and right sections of layer II. (**a**) Time evolution of local order parameters for the left (green) and right (red) sections. Frequency-filtered signals: (**b**) low-frequency oscillations (LFOs) in the range of 0.01–0.045 Hz and (**c**) middle-frequency oscillations (MFOs) in the range of 0.08–0.18 Hz. The parameters used are $\Delta\omega = 0.8$, $\lambda = 10$, and $\sigma = 2.11$.

Description of Figure SF4:

This figure illustrates that at the stationary state, all pairs of mirror nodes in the middle section are synchronized, while the phase difference between mirror nodes in the left and right sections varies periodically. This periodic variation is particularly pronounced when $\alpha = \frac{\pi}{2}$. The figure illustrates the phase similarities for all pairs of mirror nodes, defined as $S_{M_i}(t) = \cos\left(\theta_i^{II}(t) - \theta_i^{I}(t)\right)$, for $i = 1 \ldots N$. Panel (**a**) shows results for $\sigma = 0.39$, while panel (**b**) presents results for $\sigma = 2.11$. The narrow red strip in the center of both panels represents the nodes in the middle section that are synchronized with their corresponding mirror nodes. The Regular frequency assignment model was used in this analysis.

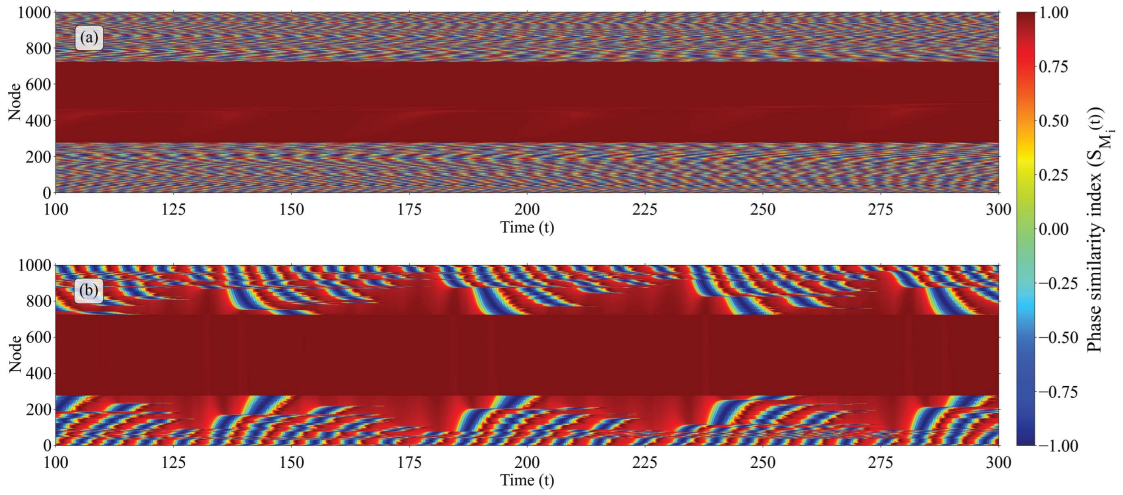

Figure SF 4: Phase similarities of mirror nodes over time, $S_{M_i}(t) = \cos\left(\theta_i^{II}(t) - \theta_i^{I}(t)\right)$, for a system with $\alpha = \frac{\pi}{2}$. Panel (**a**) displays the phase similarities for coupling within the first hysteresis loop at $\sigma = 0.39$, while panel (**b**) shows them for the second hysteresis loop at $\sigma = 2.11$. Parameters are $\Delta\omega = 0.8$ and $\lambda = 10$.

Description of Figure SF5:

Each panel shows the phase similarities of two pairs of counterpart mirror nodes, which oscillate with the same frequency. However, as the magnitude of the frequency discrepancy between the mirror nodes ($|\delta\omega|$) decreases, the frequency of their phase similarity curves also decreases, until there is no oscillation when $|\delta\omega| = 0$ in panel d. Additionally, the two curves corresponding to the counterpart pairs become in-phase as the frequency discrepancy between the mirror nodes reduces (see panels a to d for illustration).

Thus, counterpart pairs located in the middle section are synchronized (**d**). However, when these counterpart pairs are positioned in different sections (left and right), the phase similarity oscillations of their corresponding mirror nodes are out of phase (**a-c**). When $|\delta\omega|$ is at its maximum, the two counterpart phase similarity curves become anti-phase (**a**). The Regular frequency assignment model was employed in this analysis.

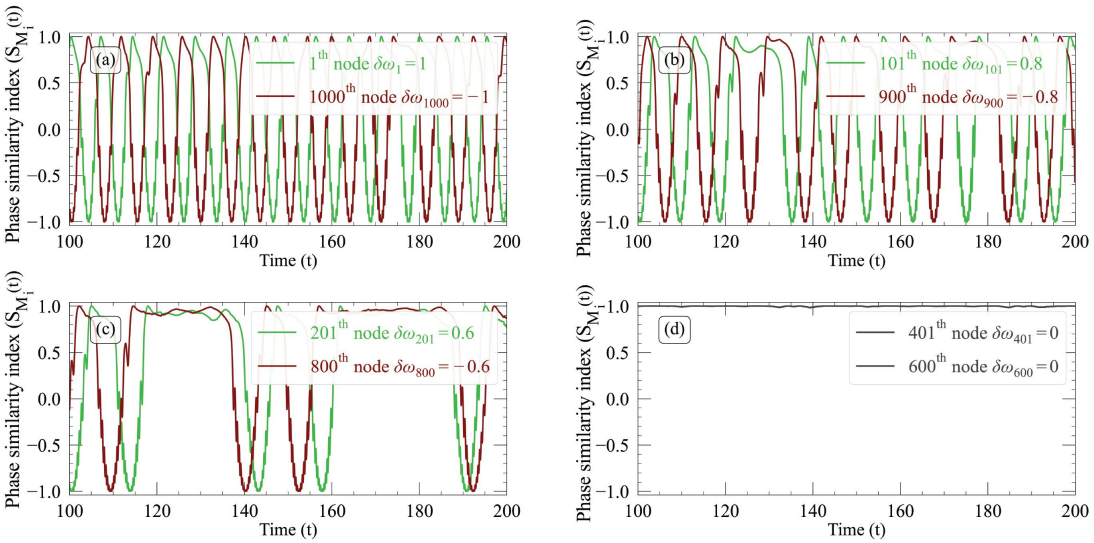

Figure SF 5: Comparison of phase similarities ($S_{M_i}(t) = \cos\left(\theta_i^{II}(t) - \theta_i^{I}(t)\right)$), where i labels mirror pairs) for four distinct pairs of counterparts. Panel (**a**) shows the phase similarities for pairs $i = 1$ and $i = 1000$; panel (**b**) for pairs $i = 101$ and $i = 900$; panel (**c**) for pairs $i = 201$ and $i = 800$; and panel (**d**) repeats the phase similarities for pairs $i = 401$ and $i = 600$. The colors green, red, and black represent the phase similarities for mirror nodes in the left, right, and middle sections of the duplex network, respectively. The parameters used are $\Delta\omega = 0.8$, $\lambda = 10$, and $\sigma = 2.11$.

Description of Figure SF6:

In our paper, we presented the results for the layer II. This figure demonstrates that partial and complete synchronization in both layers are qualitatively similar. To this end, we have plotted the synchronization order parameter for the left, middle, and right sections, as well as for the entire layer. Panel (**a**) shows the results for layer I, and panel (**b**) for layer II. The Regular model for frequency assignments was used in this analysis.

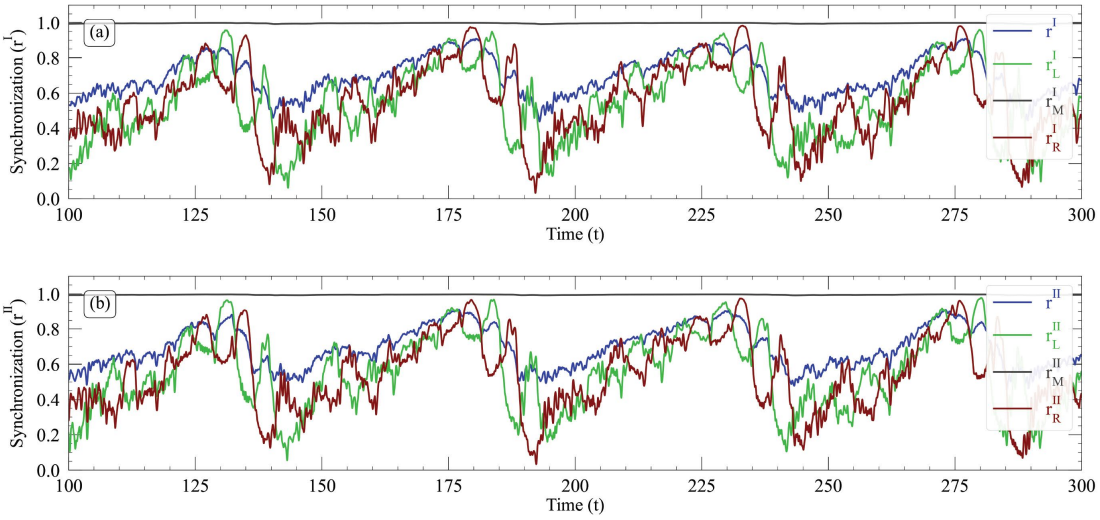

Figure SF 6: Comparison of the evolution of local and global synchronization order parameters for (**a**) layer I and (**b**) layer II. The blue line represents the synchronization of the entire layer, while the green, black, and red lines illustrate synchronization in the left, middle, and right sections of each layer, respectively. The parameters used are $\Delta\omega = 0.8$, $\lambda = 10$, and $\sigma = 2.11$.

Description of Figure SF7:

This figure investigates the temporal evolution of synchronization in the two layers of a duplex network featuring a regular frequency arrangement, where a double explosive transition is observed. The synchronization dynamics are analyzed separately for layer I (panels **a** and **b**) and layer II (panels **c** and **d**), focusing on the onset of the first ($\sigma_T^1 = 0.52$) and second ($\sigma_T^2 = 2.32$)transitions in the forward path. A notable finding is that synchronization emerges simultaneously in both layers, suggesting that interlayer synchronization develops first. These results are derived using the parameters $\alpha = \frac{\pi}{2}$, $\lambda = 10$, and $\Delta\omega = 0.8$.

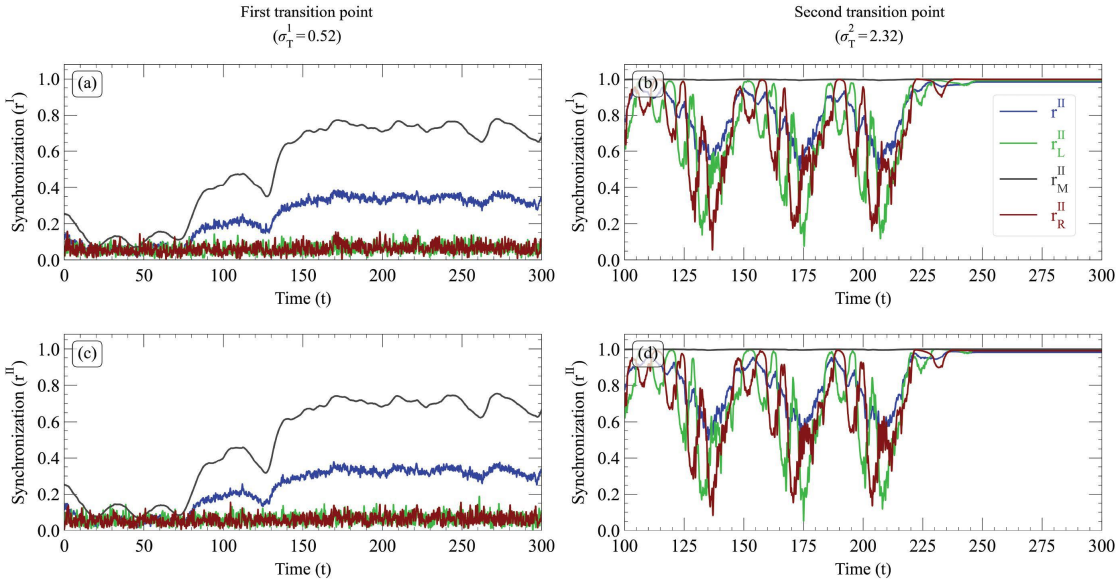

Figure SF 7: Comparison of the time evolution of synchronization order parameters in both layers of a duplex network. (**a**,**b**) Synchronization dynamics of layer I at the first and second transition points. (**c**, **d**) Synchronization dynamics of layer II at the first and second transition points. The blue, green, black, and red curves represent the order parameters for the entire layer, as well as the left, middle, and right sections, respectively. Forward synchronization is analyzed for the Regular model with $\alpha = \frac{\pi}{2}$, $\lambda = 10$, and $\Delta\omega = 0.8$.

Description of Figure SF8:

This figure demonstrates how variability in frequency differences around their mean induces an explosive phase transition in duplex networks with frustrated interlayer interactions, even when the mean frequency differences between the layers are zero. To investigate this phenomenon, we consider a scenario in which all oscillators in the first layer are assigned a fixed frequency (set to zero), while the frequencies in the second layer follow the regular model (panel **a**). This setup generates a perfectly uniform distribution of frequency differences between mirror nodes, with a mean of zero (panel **b**). Although the mean frequency difference is zero, the non-zero standard deviation of this distribution drives explosive synchronization. Additionally, the unimodal nature of the distribution leads to explosive synchronization characterized by a single hysteresis loop, even though the frequency arrangement of the nodes in the second layer is regular (panel **c**). Moreover, the synchronization of both layers occurs simultaneously and displays qualitatively similar behavior (panel **d**).

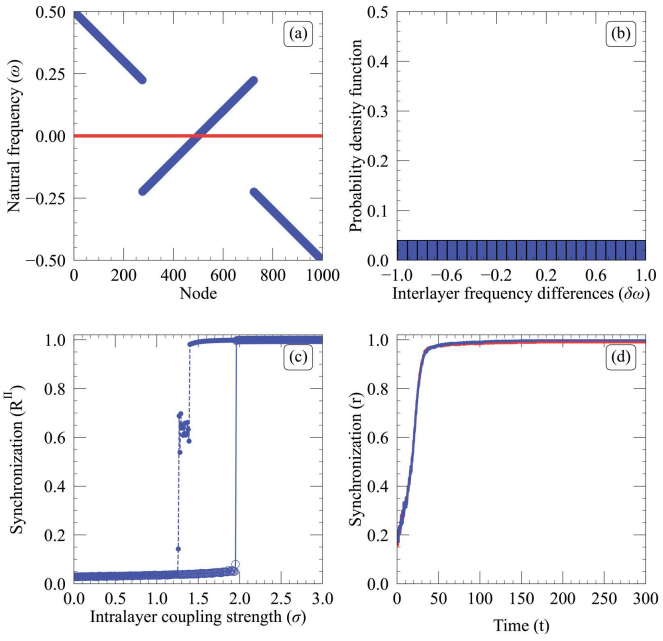

Figure SF 8: Comparative analysis of synchronization dynamics in layer II of a duplex network, where the intrinsic frequencies of layer I nodes are set to zero and the frequencies of layer II nodes follow the Regular model arrangement. (**a**) Intrinsic frequency arrangements of both layers, where layer I nodes maintain a constant frequency of zero (red), while layer II node frequencies follow the Regular model arrangement (blue). (**b**) Probability distribution function of mirror node frequency differences, demonstrating a perfectly uniform distribution. (**c**) Phase transition curve of layer II. Open markers indicate forward transitions, while filled markers represent backward transitions. (**d**) Time evolution of the synchronization order parameter for layer I (red) and layer II (blue) at the transition point of the forward path ($\sigma_T = 1.96$).

Description of Supplementary Videos

In this section, we have taken snapshots from the supplementary videos to better illustrate and explain the panels.

Description of video SV1:

The purpose of this video is to demonstrate the stationary dynamics of the duplex network with Regular frequency assignment, where $\sigma = 0$ and $\alpha = 0$. As we follow the backward paths, we observe that even when the intralayer coupling is zero, the right and left sections remain synchronized. This behavior is associated with the hysteresis loops observed in the absence of frustration.

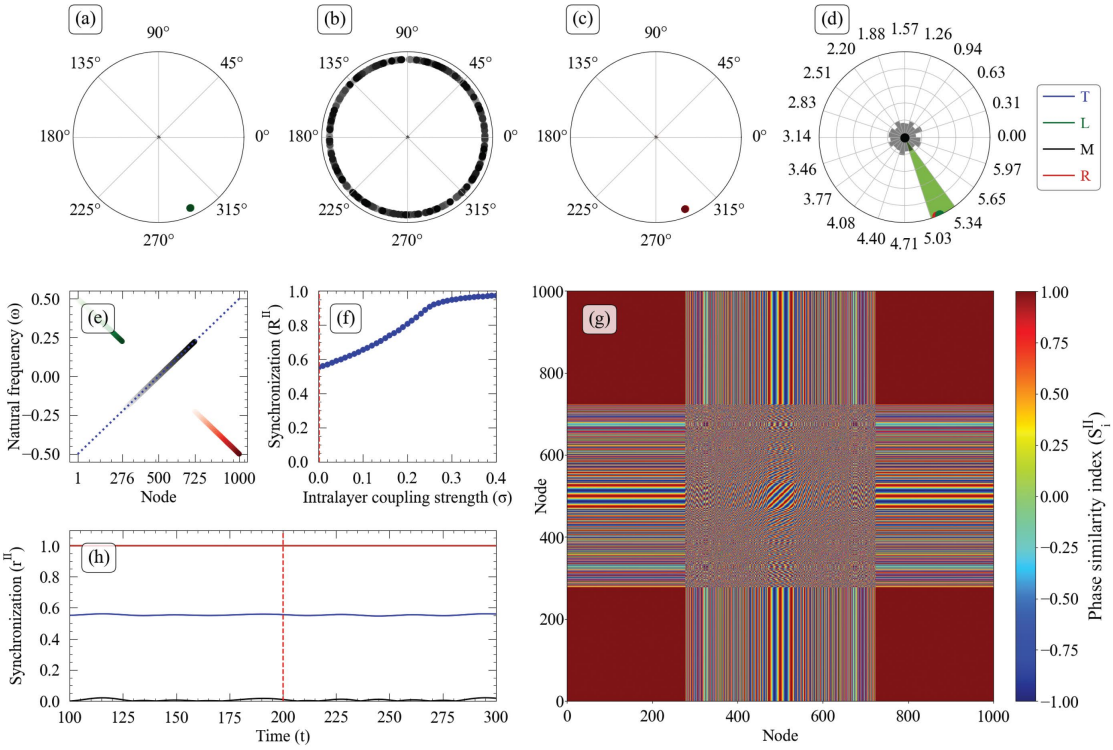

Figure SV 1: Stationary dynamics of layer II in a duplex network with zero intralayer coupling ($\sigma = 0$) and no frustration ($\alpha = 0$) under the Regular frequency assignment model. (First row): Panels (**a**–**c**) show the phase evolution of nodes on the unit circle for the left (green points), middle (black points), and right (red points) sections, with the color of the nodes becoming more intense as the node index increases within each group. Panel (**d**) displays the histogram of the nodes' phases in each group on the unit circle, with histograms for the left, middle, and right sections represented by green, black, and red, respectively. represented by its corresponding color. Panel (**e**) shows the Regular frequency arrangement of nodes in the duplex network. The blue dashed line represents the natural frequencies of the nodes in layer I, with the nodes indexed in ascending order of their frequencies. The nodes in layer II are grouped into three distinct sets, indicated by green, black, and red, corresponding to their respective frequency values. Panel (**f**) illustrates the phase transition from coherent to incoherent states along the backward path, with the red dashed line marking the intralayer coupling strength at the point of interest. Panel (**g**) shows the time evolution of the phase similarity matrix ($D_{ij}(t) = \cos(\theta_i(t) - \theta_j(t))$) at the stationary state. Panel (**h**) displays the time evolution of the synchronization order parameter for the left (green), middle (black), right (red), and entire layer (blue). The red dashed vertical line marks the time of the dynamics in the videos. All the plots presented here are plotted along the backward paths with $\Delta\omega = 0.8$.

Description of video SV2:

The purpose of this video is to showcase the periodic behavior observed in the stationary dynamics of the duplex network with Regular frequency assignment, within the first hysteresis loop, where $\sigma = 0.39$ and $\alpha = \frac{\pi}{2}$. It is evident that the periodic behavior is primarily driven by the dynamics of the middle section.

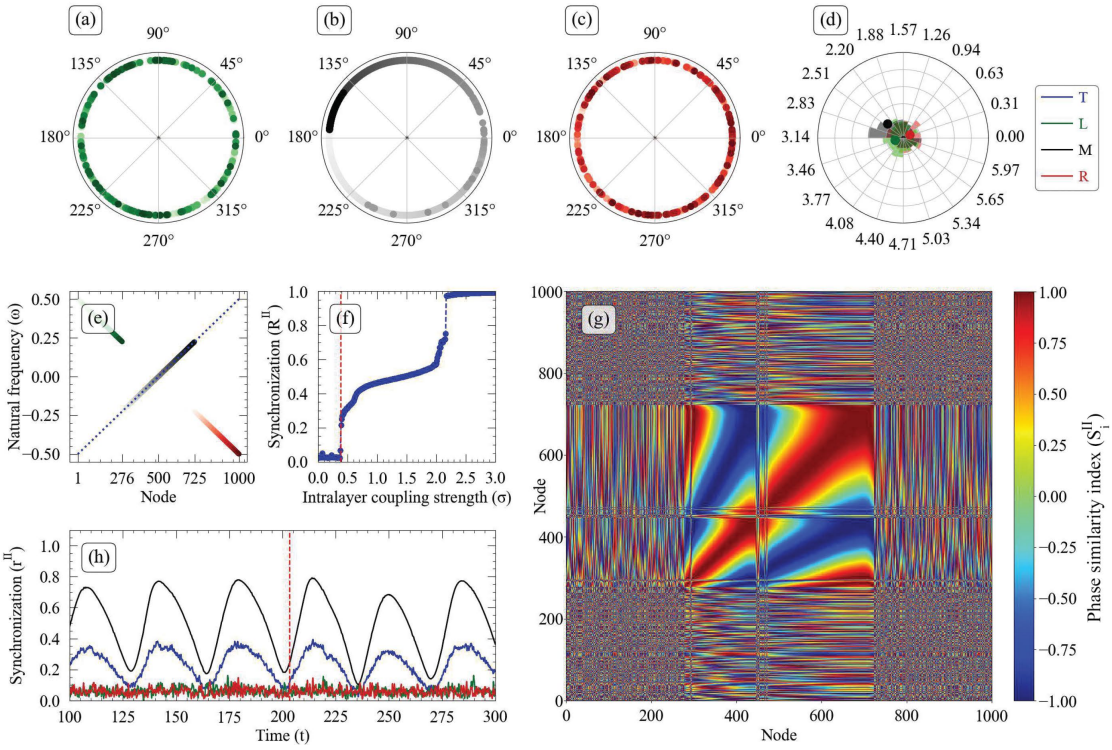

Figure SV 2: Stationary dynamics of layer II in a duplex network within the first hysteresis loop ($\sigma = 0.39$, $\alpha = \frac{\pi}{2}$) under the Regular frequency assignment model. The panel details are the same as those in supplementary video SV1.

Description of video SV3:

The purpose of this video is to demonstrate the periodic behavior observed in the stationary dynamics of the duplex network with Regular frequency assignment, within the second hysteresis loop, where $\sigma = 2.11$ and $\alpha = \frac{\pi}{2}$. The blinking process is evident in the dynamics of the left and right sections, creating a complex wave with different frequencies in the synchronization order parameter of each section.

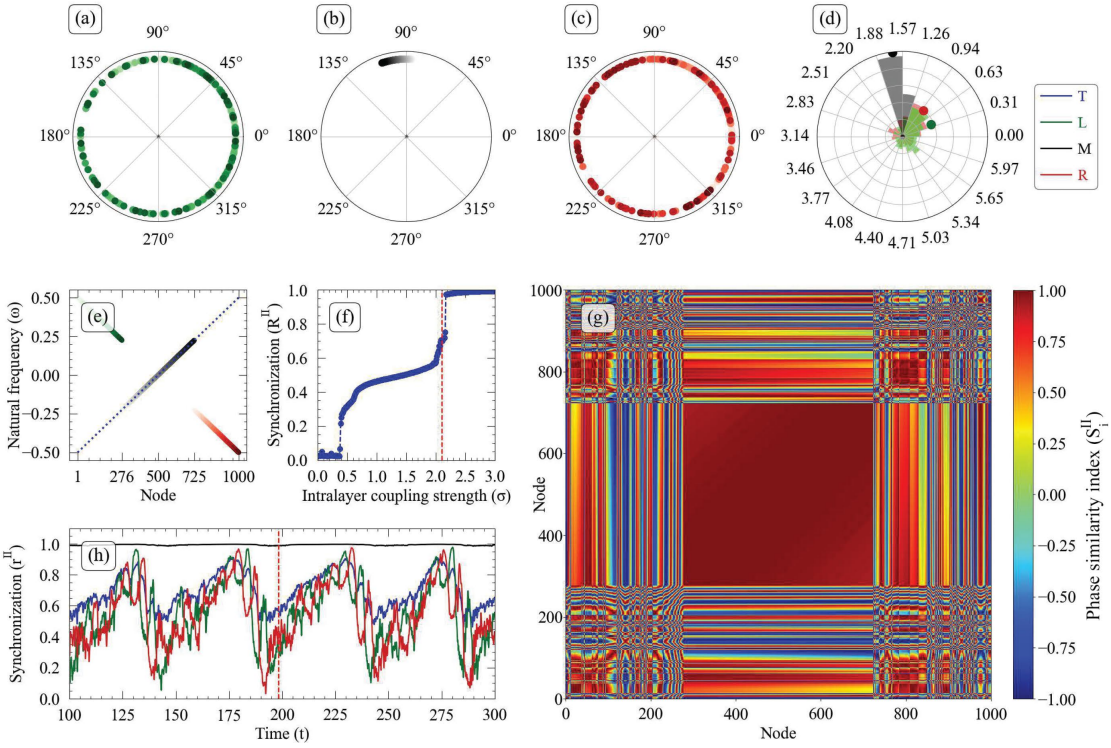

Figure SV 3: Stationary dynamics of layer II in a duplex network within the second hysteresis loop ($\sigma = 2.11$, $\alpha = \frac{\pi}{2}$) under the Regular frequency assignment model. The details of the panels are identical to those in supplementary video SV1.